Superatom State-Resolved Dynamics of the Au$_{25}$(SC$_8$H$_9$)$_{18}^-$ Cluster from Two-Dimensional Electronic Spectroscopy

Tatjana Stoll,[†] Enrico Sgrò,[†] Jeremy W. Jarrett,[‡] Julien Réhault,[†,§] Aurelio Oriana,[†] Luca Sala,[†] Federico Branchi,[†] Giulio Cerullo,[†] and Kenneth L. Knappenberger, Jr.*,[†,‡]

[†]IFN-CNR, Dipartimento di Fisica, Politecnico di Milano, Piazza Leonardo da Vinci 32, 20133 Milano, Italy
[‡]Department of Chemistry and Biochemistry, Florida State University, Tallahassee, Florida 32306-4390, United States
[§]Paul Scherrer Institute, CH-5232 Villigen PSI, Switzerland

S *Supporting Information*

ABSTRACT: Superatom state-resolved dynamics of the Au$_{25}$(SC$_8$H$_9$)$_{18}^-$ monolayer-protected cluster (MPC) were examined using femtosecond two-dimensional electronic spectroscopy (2DES). The electronic ground state of the Au$_{25}$(SC$_8$H$_9$)$_{18}^-$ MPC is described by an eight-electron P-like superatom orbital. Hot electron relaxation (200 ± 15 fs) within the superatom D manifold of lowest-unoccupied molecular orbitals was resolved from hot hole relaxation (290 ± 20 fs) in the superatom P states by using 2DES in a partially collinear pump−probe geometry. Electronic relaxation dynamics mediated by specific superatom states were distinguished by examining the time-dependent cross-peak amplitudes for specific excitation and detection photon energy combinations. Quantification of the time-dependent amplitudes and energy positions of cross peaks in the 2.21/1.85 eV (excitation/detection) region confirmed that an apparent energetic blue shift observed for transient bleach signals results from rapid hot electron relaxation in the superatom D states. The combination of structurally precise MPCs and state-resolved 2DES can be used to examine directly the influence of nanoscale structural modifications on electronic carrier dynamics, which are critical for developing nanocluster-based photonic devices.

Monolayer protected clusters (MPCs) are photonic nanoparticles spanning the sub-nm to few-nm size range that can be isolated with structural and compositional control. The optical and electronic properties of MPCs depend upon three structurally distinct components: (i) metal atom core, (ii) inorganic protecting units, and (iii) organic ligands that aid cluster dispersion in colloidal suspension. Over the past several years, advances in synthetic methodologies have enabled manipulation of MPC size, composition, and structure to achieve functionalities that include nonlinear frequency conversion,[1,2] ligand-dependent photoluminescence,[3−5] resistive magnetic-field heating,[6] and photocatalysis.[7,8]

The Au$_{25}$(SC$_8$H$_9$)$_{18}^-$ MPC is composed of a 13-gold-atom icosahedral core that is capped by 12 additional gold atoms arranged in six protecting groups formed by alternating S−Au bonds.[9,10] Thiolate ligands bridge the Au atoms of the protecting group. Based on this geometric structure, the electronic levels

structure and visible steady-state absorption spectra of a series of Au$_{25}$(SR)$_{18}^-$ clusters have been described from density functional calculations.[10−12] The electronic structure of the anionic species is understood using superatom models that place valence electrons in a spherically symmetric potential.[13] In this context, Au$_{25}$(SC$_8$H$_9$)$_{18}$ corresponds to an eight-electron system with a filled superatom P shell. The P shell consists of three nearly degenerate electronic states that form the HOMO (p$_z$), HOMO−1 (p$_{xy}$), and HOMO−2 (p$_{xy}$) orbitals localized on the 13-atom core of the cluster.[12] The visible steady-state absorption spectrum results primarily from electronic transitions from the superatom P manifold of states to various components of the superatom D levels (also localized on the cluster core), which make up the LUMO through LUMO+4 states. Transitions from ligand-based states are very significant for excitation energies higher than 2.5 eV; ligand-based transitions are also identified with computed energies spanning 1.6 and 1.8 eV, but with much smaller oscillator strengths than transitions localized to the cluster core.[12]

Femtosecond transient absorption (TA) spectroscopy techniques have been applied to study electronic relaxation for several gold MPCs.[14−18] In the case of the 25-gold-atom system, Miller et al. have identified rapid internal conversion, subsequent to excitation of core-localized transitions, which is followed by picosecond metal-to-ligand shell relaxation.[14] Green et al. used two-color femtosecond visible pump/NIR probe spectroscopy to examine the influence of MPC oxidation state on electron dynamics.[16] For the open shell charge neutral Au$_{25}$(SC$_8$H$_9$)$_{18}$ species, NIR probing revealed a few-hundred-picosecond intersystem crossing process that proceeded from excited states near the HOMO−LUMO energy gap. Models invoking splitting of HOMO−LUMO transitions have also been used to describe dynamics for Au$_{25}$ MPCs in different oxidation states.[15]

Despite these significant advances in controlled synthesis, electronic structure characterization, and extensive investigations of MPCs using 1D femtosecond TA spectroscopy, state-resolved descriptions of MPC electronic dynamics have not been achieved. We here examine for the first time electronic energy relaxation dynamics of Au$_{25}$(SC$_8$H$_9$)$_{18}^-$ clusters using femtosecond two-dimensional electronic spectroscopy (2DES) in the visible. 2DES combines high temporal and spectral resolution,

and by spreading the information content of the nonlinear signal on two frequency axes, it allows to distinguish signals that are spectrally overlapped in the 1D experiments.[19] By employing ultrabroadband sub-20 fs pulses from noncollinear optical parametric amplifiers as both the pump and probe laser pulses in the 2DES measurement, we were able to distinguish hot electron relaxation within the superatom D manifold of states from hot hole relaxation within the superatom P states. Our 2DES experimental setup, in the partially collinear pump−probe geometry using the Translating-Wedge-Based Identical Pulses eNcoding System (TWINS) pulse replication technique,[20] has been previously described in detail.[21−23] Experimental (Figure S3) and data analysis information critical to the current work is provided as SI. MPCs synthesis, isolation, and structural characterization are also described in SI.

The $Au_{25}(SC_8H_9)_{18}{}^-$ absorption spectrum is overlaid with the excitation laser pulse in Figure 1a. Based on the Figure 1a data
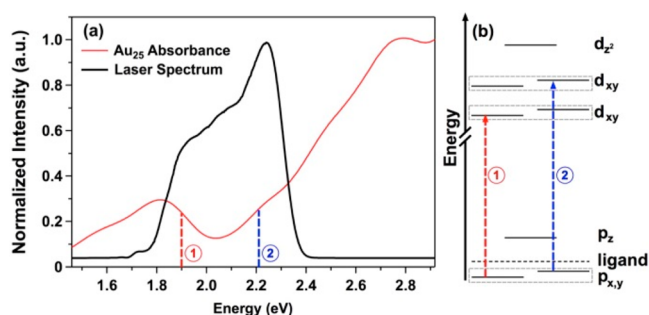

Figure 1. (a) Normalized absorbance of $Au_{25}(SC_8H_9)_{18}{}^-$ (red solid line) overlaid with the pump laser spectrum (black solid line). Specific electronic transitions are designated with vertical dashed lines. (b) Energy level diagram with transition assignments of the peaks in the linear absorption spectrum (a), as described in text.

and electronic structure calculations, the laser bandwidth spanned resonances with two distinct electronic transitions, including LUMO+3; LUMO+2 ← HOMO−1; HOMO−2 (~2.2 eV) and LUMO+1; LUMO ← HOMO−1; HOMO−2 (~1.9 eV). These two electronic transitions are depicted in Figure 1b. In contrast to previous femtosecond TA spectroscopy experiments on $Au_{25}(SC_8H_9)_{18}$ clusters, 2DES measurements can isolate the electronic relaxation dynamics of specific superatom states. This state-selectivity is observed in the 2DES absorptive maps plotted in Figures 2 and 3 for several values of the waiting time, t_2. Off-diagonal cross peaks were detected for two different excitation energies (2.21 and 1.95 eV) within the laser bandwidth. Figure 2 portrays the maps on a non-normalized intensity scale and reveals the transient signals resulted primarily from the LUMO+3; LUMO+2 ← HOMO−1; HOMO−2 transitions (2.21 eV excitation). Cross-peaks resulting from 1.95 eV excitation, corresponding to LUMO+1; LUMO ← HOMO−1; HOMO−2 pumping, are magnified by a factor of 4 in Figure 3a,b. Cross peaks were not detected for excitation energies spanning 2.0−2.1 eV. For early t_2 delay times ($t_2 \leq 150$ fs), the 2.21 eV pump-induced cross peaks consisted of multiple resolvable negative-amplitude $\Delta T/T$ excited state absorption (ESA) peaks that spanned 1.8 to 2.1 eV probe energies. At 150 fs < $t_2 \leq 500$ fs, a single, broad cross peak was detected that exhibited a time-dependent shift to higher probe energy and concomitant narrowing. In addition, a positive-amplitude $\Delta T/T$ transient corresponding to ground state bleaching (GSB) appeared at 1.85 eV detection energy for $t_2 \geq 500$ fs.
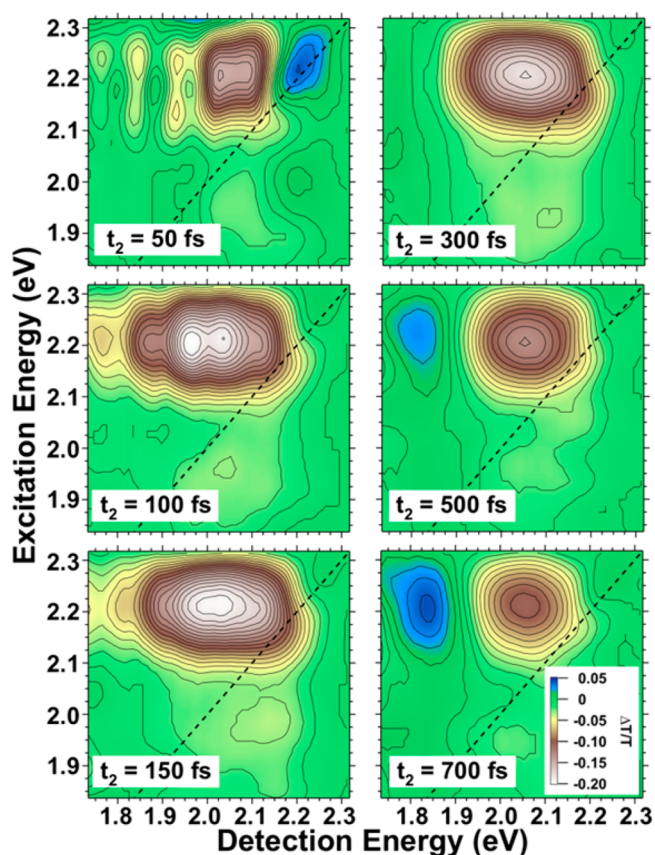

Figure 2. Absorptive 2DES maps at designated t_2 waiting times. Negative $\Delta T/T$ indicates excited state absorption, and positive signals correspond to transient bleaching. Absolute color and contour scale in all traces are set to the minimum and maximum intensity values throughout the map over the entire time series, and the color scale is displayed in the bottom right panel. The excitation pulse energy was 14 nJ.
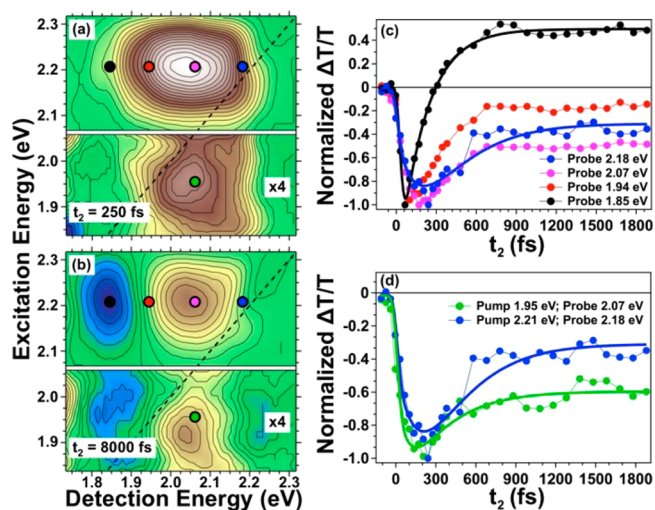

Figure 3. (a,b) Absorptive 2DES maps with the region from 1.73 to 2.07 eV multiplied by a factor of 4 to emphasize the low-pump-energy cross peak. (c,d) Extracted t_2 dynamics from the regions identified by the colored markers in (a,b). All panel (c) data resulted from 2.21 eV excitation. Solid lines are fits to a double exponential convolved with a Gaussian instrument response with 35 fs fwhm. The excitation pulse energy was 14 nJ.

In order to examine quantitatively the time-dependent effects shown in Figure 2, cross-peak signal amplitudes resulting from 2.21 eV excitation were compared versus t_2 delay time for several detection energies (Figure 3c). The 1.85 eV signal, the lowest detection energy shown in Figure 3c (black filled circles), exhibited prompt negative amplitude, reflective of ESA. The sign of this signal inverted from negative to positive amplitude (GSB) with a first-order time constant of 200 ± 7 fs and then persisted at constant amplitude for the remainder of the t_2 scan. The observation of GSB at 1.85 eV is consistent with expectations based on the energy for the broad LUMO+3; LUMO+2 ← HOMO−1; HOMO−2 peak detected by linear absorption (Figure 1). The prompt negative amplitude $\Delta T/T$ signal was approximately 250% larger than the positive amplitude signal that persisted for long t_2 times. The sign reversal of the 1.85 eV transient signal could be understood from the time dependence of the 2DES signal detected at higher energies. In contrast to the 1.85 eV probe data, cross peaks detected at 1.94, 2.07, and 2.18 eV all showed a first-order buildup of signal amplitude that increased from 15 ± 5 fs (1.94 eV) to 200 ± 15 (2.18 eV) and a probe-energy-independent decay time constant of 290 ± 20 fs; see Figure 3 and Table S1 for fitting results. These time constants were independent of excitation pulse energy over the experimental ranges that spanned 5 to 20 nJ. The time-dependent behavior of the 2DES cross peak amplitudes is consistent with internal electronic conversion from high-energy to lower-energy excited electronic states. Taken together, the close correspondence of the time constants for signal change of sign at 1.85 eV probe and the growth of the 2.18 eV probe signals along with the large difference between negative and positive $\Delta T/T$ signal amplitudes detected at 1.85 eV indicate that the perceived growth of the transient bleach signal resulted from the rapid decay of intense ESA that overwhelmed the GSB signal at early t_2 time delays. Therefore, these 2DES data indicate that previous observations[15] of time-dependent blue shifts of GSB signals for $Au_{25}(SC_8H_9)_{18}$ clusters, as shown in Figure S4, resulted from time-dependent decay of overlapping ESA and GSB signals that congested the TA spectra.

In order to assign the electronic relaxation dynamics of $Au_{25}(SC_8H_9)_{18}$ MPCs to specific superatomic states, the cross peak dynamics resulting from 2.21 and 1.9 eV excitation are compared in Figures 3a,b. In contrast to 2.21 eV excitation, cross peaks detected along the 1.9 eV pump axis did not exhibit a time-dependent shift to higher probe energies. The time-dependent cross-peak amplitudes from these two different excitation photon energies are compared in Figure 3d. The growth time constant of the 1.95 eV/2.07 eV pump/probe cross peak was accelerated (85 ± 15 fs) compared to the 2.21 eV/2.18 eV data (200 ± 15 fs). The 1.95 eV/2.07 eV pump/probe signal decayed with a 310 ± 35 fs time constant that matched the 2.21 eV/2.18 eV result within error. Therefore, analysis of the cross-peak amplitudes on time scales shorter than 200 fs isolated differences in the electronic relaxation dynamics for the $Au_{25}(SC_8H_9)_{18}$ MPC that, to date, have not been resolved using conventional 1-D TA spectroscopy techniques. A kinetic model describing the observed dynamics is given in Figure 4. A 2.21 eV-pumping generates a hot electron with excitation in excess of the LUMO energy by approximately 250 meV. In contrast, the 1.95 eV pump promotes the electron to the nearly degenerate LUMO and LUMO+1 states. Both pump energies form hot holes in HOMO−1 and HOMO−2 levels located approximately 130 meV below the MPC HOMO.[11] Therefore, the differences detected in the cross peak widths and time-dependent
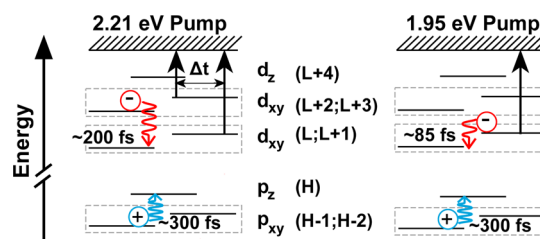

Figure 4. Model of relaxation for electrons and holes following 2.21 eV (left) and 1.95 eV excitation (right).

amplitudes for early t_2 times (<200 fs) are attributed to relaxation of electrons through the manifold of states making up the superatomic D orbitals of the $Au_{25}(SC_8H_9)_{18}$ MPC. Following 2.21 eV excitation, hot electrons created in the LUMO+2 and LUMO+3 states rapidly internally convert to the LUMO level within 200 fs. Cross-peak detection using visible probe pulses gives an ESA signal, resulting from exciting these hot electrons into a high-energy continuum of excited states within the Au sp conduction band.[12] As the hot electrons relax to the LUMO level, more energetic probe energies are required to project these carriers into the continuum, giving rise to the observed blue-shift of the ESA peak and uncovering the GSB signal at lower energies. The time-dependent cross-peak width and central position are plotted selecting 2.21 eV as the excitation energy in Figures S4 and S5. The combined time-dependent 65 meV peak shift and 170 meV narrowing are in good agreement with the approximately 250 meV gap separating the LUMO+2; LUMO+3 and LUMO; LUMO+1 excitation energies. The close agreement between the shift in probe detection and excess excitation energies resulting from 2.21 eV pumping support this interpretation for the time dependence of the cross peak data. Excitation using 1.95 eV promotes an electron to the LUMO and LUMO+1 states. The rapid 85 fs component is attributed to internal conversion of the electron from the LUMO+1 to LUMO level. The differences in these time constants can be understood from the energy-gap law for nonradiative electronic relaxation, which predicts the time constants to increase concomitantly with the energy separation between initial and final electronic states.[24] The 300 fs cross peak decay, which was common to both 2.21 and 1.95 eV pumping, is attributed to internal conversion of holes between the HOMO−2 and HOMO states. The nondecaying, but nonzero, cross peak amplitudes detected for longer t_2 time delays result from electron−hole pairs formed by the superatom D and superatom P states that relax on time scales longer than those considered here.[14]

In conclusion, we have presented the first 2DES study of a structurally precise monolayer-protected cluster, which allowed for electron dynamics of the $Au_{25}(SC_8H_9)_{18}$ Superatom P and D states to be resolved, which has not been possible using conventional 1-D methods. Our results show that hot electrons thermalize within the manifold of d_{xy} superatom D states within 200 fs. Hot holes formed by visible excitation exhibit slower electronic relaxation within the superatom P manifold of states in fewer than 300 fs. Through analysis of dependence of cross-peak amplitudes on t_2 delay, we determined that $Au_{25}(SC_8H_9)_{18}$ transient absorption spectra consist primarily of excited state absorption from the superatom D state to higher energy states. The subsequent 200 fs electron internal conversion process resulted in an energetic blue shift of the ESA signal and the delayed detection of transient GSB of transition from the HOMO−1; HOMO−2 states. This observation, made possible

by 2DES, resolves the mechanism for the apparent time-dependent blue shift of the transient bleach signal. The state-specificity afforded by femtosecond 2DES for studying MPC electron dynamics will provide an important diagnostic for establishing the structure–photonic function interplay of the structurally precise class of colloidal nanoparticles.

ASSOCIATED CONTENT

Supporting Information

The Supporting Information is available free of charge on the ACS Publications website at DOI: 10.1021/jacs.5b12621.

> Synthesis, experimental setup for 2DES, data fitting procedure, and additional supplementary figures (PDF)

AUTHOR INFORMATION

Corresponding Author

*kknappenberger@fsu.edu

Notes

The authors declare no competing financial interest.

ACKNOWLEDGMENTS

REFERENCES

(1) Knoppe, S.; Vanbel, M.; van Cleuvenbergen, S.; Vanpraet, L.; Burgi, T.; Verbiest, T. *J. Phys. Chem. C* **2015**, *119*, 6221.

(2) Philip, R.; Chantharasupawong, P.; Qian, H.; Jin, R.; Thomas, J. *Nano Lett.* **2012**, *12*, 4661.

(3) Parker, J. F.; Fields-Zinna, C. A.; Murray, R. W. *Acc. Chem. Res.* **2010**, *43*, 1289.

(4) Wu, Z.; Jin, R. *Nano Lett.* **2010**, *10*, 2568.

(5) Green, T. D.; Yi, C.; Zeng, C.; Jin, R. C.; McGill, S.; Knappenberger, K. L., Jr. *J. Phys. Chem. A* **2014**, *118*, 10611.

(6) McCoy, R. S.; Choi, S.; Collins, G.; Ackerson, B. J.; Ackerson, C. J. *ACS Nano* **2013**, *7*, 2610.

(7) Tsunoyama, H.; Ichikuni, N.; Sakurai, H.; Tsukuda, T. *J. Am. Chem. Soc.* **2009**, *131*, 7086.

(8) Li, G.; Jin, R. C. *Acc. Chem. Res.* **2013**, *46*, 1749.

(9) Heaven, M. W.; Dass, A.; White, P. S.; Holt, K. M.; Murray, R. W. *J. Am. Chem. Soc.* **2008**, *130*, 3754.

(10) Zhu, M.; Aikens, C. M.; Hollander, F. J.; Schatz, G. C.; Jin, R. *J. Am. Chem. Soc.* **2008**, *130*, 5883.

(11) Aikens, C. M. *J. Phys. Chem. Lett.* **2010**, *1*, 2594.

(12) Aikens, C. M. *J. Phys. Chem. Lett.* **2011**, *2*, 99.

(13) Walter, M.; Akola, J.; Lopez-Acevedo, O.; Jadzinsky, P. D.; Calero, G.; Ackerson, C. J.; Whetten, R. L.; Groenbeck, H.; Hakkinen, H. *Proc. Natl. Acad. Sci. U. S. A.* **2008**, *105*, 9157.

(14) Miller, S. A.; Womick, J. M.; Parker, J. F.; Murray, R. W.; Moran, A. M. *J. Phys. Chem. C* **2009**, *113*, 9440.

(15) Qian, H.; Sfeir, M. Y.; Jin, R. *J. Phys. Chem. C* **2010**, *114*, 19935.

(16) Green, T. D.; Knappenberger, K. L., Jr. *Nanoscale* **2012**, *4*, 4111.

(17) Yi, C.; Tofanelli, M. A.; Ackerson, C. J.; Knappenberger, K. L., Jr. *J. Am. Chem. Soc.* **2013**, *135*, 18222.

(18) Yi, C. Y.; Zheng, H. J.; Tvedte, L. M.; Ackerson, C. J.; Knappenberger, K. L. *J. Phys. Chem. C* **2015**, *119*, 6307.

(19) Mukamel, S. *Annu. Rev. Phys. Chem.* **2000**, *51*, 691.

(20) Brida, D.; Manzoni, C.; Cerullo, G. *Opt. Lett.* **2012**, *37*, 3027.

(21) Réhault, J.; Maiuri, M.; Manzoni, C.; Brida, D.; Helbing, J.; Cerullo, G. *Opt. Express* **2014**, *22*, 9063.

(22) Réhault, J.; Maiuri, M.; Oriana, A.; Cerullo, G. *Rev. Sci. Instrum.* **2014**, *85*, 123107.

(23) Maiuri, M.; Réhault, J.; Carey, A. M.; Hacking, K.; Garavelli, M.; Luer, L.; Polli, D.; Cogdell, R. J.; Cerullo, G. *J. Chem. Phys.* **2015**, *142*, 212433.

(24) Freed, K. F.; Jortner, J. *J. Chem. Phys.* **1970**, *52*, 6272.